

RESEARCH

Open Access



# Bidirectional approach of *Punica granatum* natural compounds: reduction in lung cancer and SARS-CoV-2 propagation

Md. Abul Barkat<sup>1</sup>, Afreen Fatima<sup>2</sup>, Bushra Riaz<sup>2</sup>, Mohd. Zaheen Hassan<sup>3</sup>, Tanveer Ahamad<sup>4</sup>, Abdulkareem A. Alanezi<sup>1</sup>, Harshita Barkat<sup>1</sup>, Afaf F. Almuqati<sup>5</sup>, Yahya I. Asiri<sup>6</sup> and Sahabjada Siddiqui<sup>4\*</sup>

## Abstract

The spreading of COVID-19 has posed a risk to global health, especially for lung cancer patients. An investigation is needed to overcome the challenges of COVID-19 pathophysiology and lung cancer disease. This study was designed to evaluate the phytoconstituents in *Punica granatum* peel (PGP), its anti-lung cancer activity, and in silico evaluation for antiviral potential. GC–MS technique was used to detect the phytoconstituents. Cytotoxicity was analyzed using MTT dye, followed by apoptosis, ROS generation, and cell cycle phase detection in human lung cancer cells (A549). The glide module of Maestro software was used to investigate the molecular-docking interaction of the constituents against main protease (Mpro) and papain-like protease (PLpro) of SARS-CoV-2. GROMACS 2023.2 was utilized to evaluate the complex stability. A total of nineteen phytocomponents were detected in the PGP extract through GC–MS analysis. PGP has shown a potential to reduce lung cancer cell proliferation while evading normal cell death. PGP induced apoptosis by arresting cells in the G0/G1 phase and generating ROS. A total of six and eight phytocomponents had a high affinity for PLpro and Mpro proteins, respectively. The top docked complex, ethyl 5-oxo-2-pyrrolidinecarboxylate, with PLpro and Mpro proteins, showed likely stable interaction throughout 100 ns simulation. This finding raises the possibility of top-eight hits (docking score  $\geq -1.0$  kcal/mol) preventing SARS-CoV-2 severity. The phytoconstituents exhibited orally active drugs with no more than one violation and drug-likeness activity. The PGP phytoconstituents are suggested to be dual agents for lung cancer and SARS-CoV-2 pathogenesis.

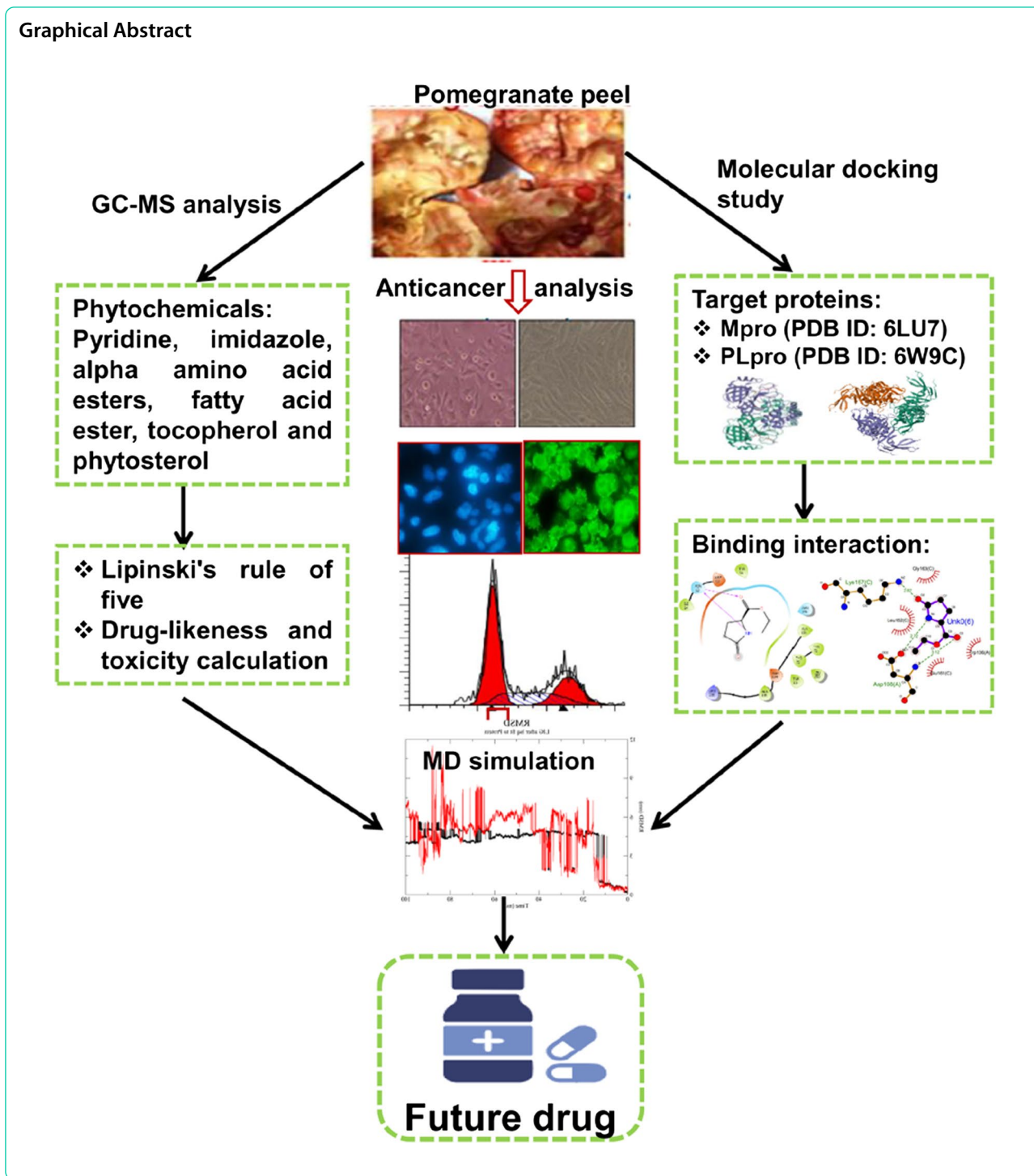
**Keywords** Phytochemical analysis, COVID-19, Lung cancer, *Punica granatum* peel, Molecular docking

\*Correspondence:  
Sahabjada Siddiqui  
sahabjadabiotech04@gmail.com

Full list of author information is available at the end of the article



© The Author(s) 2025. **Open Access** This article is licensed under a Creative Commons Attribution-NonCommercial-NoDerivatives 4.0 International License, which permits any non-commercial use, sharing, distribution and reproduction in any medium or format, as long as you give appropriate credit to the original author(s) and the source, provide a link to the Creative Commons licence, and indicate if you modified the licensed material. You do not have permission under this licence to share adapted material derived from this article or parts of it. The images or other third party material in this article are included in the article's Creative Commons licence, unless indicated otherwise in a credit line to the material. If material is not included in the article's Creative Commons licence and your intended use is not permitted by statutory regulation or exceeds the permitted use, you will need to obtain permission directly from the copyright holder. To view a copy of this licence, visit <http://creativecommons.org/licenses/by-nc-nd/4.0/>.



**Introduction**

Currently, efforts are being made around the globe to protect people from a coronavirus disease (COVID-19) caused by SARS-CoV-2 which was found at the end of 2019 in the Chinese province of Wuhan [1]. Cancer patients are extremely susceptible due to frequent

interactions with the health system, weakened immune systems or treatments using drugs like steroids, and most crucially, advanced age and comorbidities [2]. Comparing SARS-CoV-2 infection to other cancers, patients with lung cancer and those who have hematological malignancies seem to be at the highest risk of dying from the

infection [3]. There were 23 patients with a history of lung cancer in the largest report from China, a multicenter retrospective cohort study with 13,077 patients with COVID-19, albeit only five had metastatic lung cancer. In this category, 39% of patients died, and 78% of patients had a serious clinical outcome [4]. In general, this series demonstrated that cancer patients were more expected to experience grievous sickness. A combination therapy of herbal supplements with standard drugs is an alternative approach that could be used to improve patient outcomes. A strong strategy is also needed to prevent SARS-CoV-2 from emerging shortly due to seasonal variation and various mutations of SARS-CoV-2, which has been a major worldwide problem in treating the virus [5]. Similar to earlier pandemics, it has been demonstrated that the development of potent medications could offer a long-term remedy for COVID-19 [6]. Therefore, herbal compounds could be investigated in the development of potent medicines since they may offer advantages in terms of accessibility, affordability, and convenience of use.

Herbal products have advantages in terms of scaffold diversity and structural complexity, which may be useful in drug-disease interactions. Besides, numerous natural products have been proven to exert antiviral effects, including HIV, dengue viruses, coronaviruses, and hepatitis viruses [7, 8]. Selection of potential herbs is very important in the development of effective drugs to combat SARS-CoV-2 illness, and thus far several studies have reported the effectiveness of a few herbs in inhibiting SARS-CoV-2 propagation [9]. Among the herbal plant species, *Punica granatum*, also known as Pomegranate, has shown promising pharmacological and medicinal values. Several classes of bioactive compounds, such as alkaloids, tannins, anthocyanins, phenolics, proanthocyanidins, flavonoids, steroids, terpenes and terpenoids, fatty acids and organic acids, xanthonoids, lignans, and vitamin C, are abundant in Punica fruits [10]. The seeds, juice, and peel parts of the fruit are used for beverages and jams and have provided health and nutritional benefits as well as therapeutic benefits [9, 10]. Previous studies have shown various medicinal values such as antimicrobial, antioxidant, anti-inflammatory and anticarcinogenic activities in addition to cardiac, lung and liver protection [11–13]. In a previous study, Punica peel extract, its fraction, and the active compound punicalagin have shown virucidal activities against the mosquito-borne Mayaro virus [14]. In addition, Punica juice has provided an HIV-1 entry inhibition and topical microbicide [15]. In a previous study, Punica peel extract effectively inhibited the growth of fungi *A. niger*, *P. italicum*, *R. mucilaginosa* and also showed antimicrobial activity against both Gram +ve and Gram -ve bacteria strains [16, 17].

Based upon the above report, the present study has focused on analyzing the phytochemicals in pomegranate peel extract and their cytotoxic activity in human lung carcinoma A549 cells as well as exploring the antiviral effects through computational molecular docking and molecular dynamics (MD) simulation analysis. The peel part of Punica (var. Jalore seedless), procured from Jodhpur, India, was studied by Gas chromatography-mass spectrometry (GC–MS) to determine the phytochemistry in the extract due to the distinct geography and soil profile. In the current study, two protein targets namely papain-like protease (PLpro) and main protease (Mpro) were selected because these are essential for viral replication. The coronavirus Mpro plays a key role in enzymatic activity in its post-translational processing of replicase polyproteins [18]. PLpro is involved in converting viral polyproteins into functional proteins and plays a crucial part in the host's defense mechanism [19]. Thus, focusing on these particular targets of SARS-CoV-2 and inducing lung cancer cell death may establish a reasonable strategy for developing and discovering antiviral and anti-lung cancer therapeutics.

## Materials and methods

### Source of plant material and identification

Jalore seedless variety of pomegranate fruits was purchased in February from a reputed supplier in Jodhpur, India. Fruit samples were identified and submitted in the Pharmacognosy Section, Integral University, Lucknow (F.No. IU-PHAR-HRB-14–08).

### Ethanol extract preparation

The ethanolic extract was prepared as per the previous method [20]. In brief, peeled parts of pomegranate fruits were separated, rinsed in ddH<sub>2</sub>O, air-dried in shadow and then the powder was made with the help of a Bajaj grinder (GX15, India). The grinded powder was soaked in 95% ethanol for 3 days at room temperature and soluble components were extracted using the maceration process. Supernatants were placed on the filter membrane (Whatman No. 1) to separate the filtrate and ethanol was evaporated with the help of a Rotatory evaporator. The obtained semi-solid paste was evaporated further in a water bath to get a semi-dried form of PGP extract. This extract was used for phytochemical study, in vitro toxicity tests, and in silico investigation.

### GC–MS analytical technique

The chemical characterization of 95% PGP extract was performed by GC–MS-QP2010 Plus system (Shimadzu, Japan) and capillary column RTX-5 MS (Restek, United States) from Central Research Facility, JNU, New Delhi as per a previous study [21]. Plant extract with many

constituents were separated into their components at their retention times through GC and the mass spectrophotometer provided a mass spectrum to characterize the components. A chromatogram indicating the relative abundance or quantity of each component as a function of retention time was created by the software of a mass spectrophotometer. Mass spectra of unidentified components were compared to the spectra of identified components kept in the chemistry libraries NIST08s and WILEY8.LIB.

#### **Cytotoxicity assay through MTT dye**

Human lung carcinoma A549 cells and normal Vero cell line of kidney origin were procured from NCCS, Pune, India. Both cell lines were cultured in DMEM-F12 media and maintained at 37 °C with 5% CO<sub>2</sub> in an incubator (Eppendorf, USA). Both cell lines at density 1 × 10<sup>4</sup> cells per well in 200 µL DMEM-F12 media were seeded in a 96-well culture plate for overnight incubation at cultured condition. To find the proper doses of 25, 50, 100, and 250 µg/mL, a stock solution of pomegranate peel was prepared and diluted in complete growth media and treated in triplicate for 24 h. After incubation, media was removed and 100 µL (stock solution 5 mg/mL) of MTT reagent was added and further incubated for 3–4 h for the development of blue crystals. Now, the MTT solution was replaced with 100 µL DMSO solution. A microplate reader (BIORAD-PW41, USA) was operated to measure the absorbance of the solubilized color product at 540 nm and the percentage of cell viability was determined [20].

#### **Apoptosis and ROS generation assay**

DAPI is a fluorescent nuclear marker used to analyze the apoptotic effect of PGP extract. Cells were treated at two effective doses 50 and 100 µg/mL for 24 h and were fixed then in paraformaldehyde solution. Images were captured following DAPI staining under an inverted fluorescent microscope (Nikon ECLIPSE Ti-S, Japan). Further, to check whether ROS is the potential causative agent for cell death, ROS generation was also evaluated as per the established method using DCFHDA dye [22]. In brief, for imaging analysis, cells were exposed to PGP extract at 50 and 100 µg/mL in 96-well plate for 12 h following 10 µM DCFH-DA dye staining. Images were captured using a fluorescent microscope. For quantitative analysis, approx. 1 × 10<sup>4</sup> cells/well were cultured overnight in 96-well black bottom culture plate. Following treatment, cells were incubated in DCFH-DA dye for 30 min and it was replaced with 200 µL PBS. Reading was measured at 485/528 nm of excitation/emission wavelength using a multiwell plate reader (BioTek's Synergy H1 Hybrid Multi-Mode Microplate Reader).

#### **Cell cycle analysis**

DNA content analysis at different phases was carried out through a flow cytometer using a previously established protocol [22]. A549 cells were plated and treated for 24 h into a 6-well plate. Cultured cells were then processed as per the established protocol and four distinct phases were measured through BD FACS Calibur flow cytometer. Data were analyzed with the help of Cell Quest Pro V 3.2.1 software.

#### **Computational study**

##### ***Preparation of phytoconstituents for molecular docking***

The two-dimensional configuration of nineteen phytochemicals from PGP and standard compound hydroxychloroquine (HCQ) were retrieved from the PubChem database into SDF format. These are converted into a three-dimensional configuration through the LigPrep module of Schrödinger Maestro v2020-2. OPLS 2005 was utilized to add hydrogen atoms, tautomer generation, charged groups neutralization, ionization states, structure filtration and geometry optimization. Epik module was utilized to ionize ligands at pH 7.0 ± 2.0, which generated tautomers, desalt them, and one low energy ring confirmation was carried out for each ligand [23].

##### ***Protein preparation***

Mpro (PDB ID: 6LU7) is a homo 2-mer—A2 protein and PLpro (PDB ID: 6W9C) is a homo 3-mer—A3 protein. A protein data bank was used to retrieve the crystal structure of both proteins in.pdb format. The X-ray diffraction resolution value of Mpro and PLpro was 2.16 and 2.70 Å without any mutation. The side-chain OH group, Asn, Gln, and His states were optimized through OPLS 2005 force field by assigning bond order, substituting absent disulfide bonds and H-atoms, and clearing water molecules that were within five of the heteroatoms [24].

##### ***Preparation of receptor grid***

The interaction grid formation between phytomolecules and targeted proteins was made through receptor grid generation. The position of the docked ligand was restricted to the enclosing box, a smaller size than the workspace ligand and the centroid of the docked pose. The initial bounded ligand was omitted from the generation of the grid. The resolution of the receptor grid box was centered at coordinates 27.83, 27.83, and 27.83 Å, which correspond to the x, y, and z-axis, respectively [24].

##### ***Glide docking analysis through standard precision (SP) mode***

The glide SP flexible ligand mode was utilized to dock between ligand and protein with 10 poses per ligand using Schrödinger Maestro Release 2020-2 (SERVER

PDDL 2cf05d399450 27,008) [25]. In glide SP flexible docking analysis, the OPLS3e force field was documented. Energy-minimizing poses were executed, and the docking score was used for final scoring. For each ligand, the best-docked orientation and the lowest docking score were noted. The ranking of phytoconstituents was then determined by their docking scores, which reflect the binding energies. Best docking results with binding patterns were further investigated through LigPlot + v.2.2 software.

#### **Analysing and visualization of docking results**

After glide docking analysis using SP mode, data were obtained in the form of docking score and glide energy. Based on the docking score, top-ranking components were sorted to find the best binding interacting complex. Further, the SP visualizer was used as a ligand interaction tool to display and analyze the 2D interaction with best poses namely hydrogen bond interaction, hydrophobic interactions, and  $\pi$ - $\pi$  interactions. The best binding pattern was further examined using the program LigPlot + v.2.2.

#### **MD simulation for complex stability**

The best-docked complex was analyzed using MD simulation [26]. The SwissParam (<http://www.swissparam.ch/>) programs were used to create equivalent topology and coordinate files in.gro format, which are compatible with the CHARMM36 all atoms force field used for GROMACS running. Topology and coordinate data for the protein were generated using the pdb2gmx procedure of GROMACS 2023.2. A triclinic box was filled using TIP3P water molecules and a 1 nm gap was maintained between the solute and the walls of the box. Energy reduction was performed using the descent technique, with a maximum of 50,000 steps for each system and a convergence threshold of 100.0 kJ per mole per nm. The physiological conditions were then adjusted to 310 K and 1 bar of pressure, and two equilibration steps were carried out, each comprising 1000 ps. The constant temperature-volume (NVT) ensemble was used for the first step, and the constant temperature–pressure (NPT) ensemble was used for the second. The MD simulation run's integration duration was 2 fs, and the particle velocities were rescaled using the Berendsen thermostat algorithm. Plotting was done for many metrics, including solvent-accessible surface area (SASA), root mean square fluctuation (RMSF), radius of gyration (Rg), root mean square deviation (RMSD), H-bonds, and total interaction energy. Xmgrace 5.1.25 was used to create the graphs and figures [27].

#### **Drug-likeness characteristics**

The drug-likeness of the top eight phytoconstituents of PGP was investigated using Lipinski's rule of 5 [28]. Various significant molecular properties of drug-likeness including the number of hydrogen bond donors, topological polar surface area (TPSA), hydrogen bond acceptor sites, number of rotatable bonds, MW, and logP were calculated. Molinspiration cheminformatics software was utilized to evaluate the drug-likeness of eight active molecules.

#### **Analysis of toxicity potential of phytochemicals**

The basic knowledge of the physicochemical and toxicological properties of biomolecules is required to be optimized. At an early stage, predicting differing qualities of phytoconstituents in lead identification and development is very crucial. OSIRIS Data Warrior V5.2.1 (<https://openmolecules.org/datawarrior/download.html>) software was used to predict physicochemical and toxicological molecular properties namely drug-likeness, reproductive, tumorigenic, mutagenic, and irritating properties [20].

#### **Statistical analysis**

All biological data is shown as the mean  $\pm$  SD of three distinct experiments. Using Graph Pad Prism software (Version 5.01), the one-way analysis of variance and Dennett's multiple comparison tests were used to assess the statistical differences between the various groups. P values less than 0.05 were regarded as statistically significant differences.

## **Results and discussion**

#### **GC–MS characterization of PGP**

Due to their capacity to treat various acute and chronic illnesses, traditional medicinal herbs are generally considered safe in the medical community. In medicinal chemistry, it is important to determine the nature of chemical constituents and their phytomedicinal characteristics. With this approach, the traditional applications and medical benefits of various plant components might be established and scientifically validated. Mass spectra of single metabolites in crude extract can be very useful in molecular mass identification and clues about molecular structure, as demonstrated by an earlier study in the case of *Mediterranean propolis* [29]. While MS is used to detect the elemental profile and is a plot of the ion signal as a function of ratio and chemical structure. The volatile and thermally stable components are separated using GC. GC–MS analysis is utilized for investigating naturally occurring volatile components, and it can also

be used to investigate semi- or non-volatile components that can be converted into volatile via derivatization. Many semi- and non-volatile metabolites, namely flavonoids, sugars, sugar phosphates, sugar alcohols, lipids, organic acids, alkaloids, long-chain alcohols, amino acids, peptides, amides, and amines can also be studied by employing efficient derivatization methods involving acylation, silylation, or alkylation reactions [30, 31]. Silylation techniques were used to identify and classify the semi-volatile and non-volatile PGP extract components. The GC–MS chromatogram showed nineteen peaks *i.e.* nineteen components in native PGP alcoholic extract. The PGP extract's total ion current (TIC) chromatogram is shown in Fig. 1. Table 1 lists the detected phytochemicals from the native PGP alcoholic extract along with their percent peak area, retention time and molecular weight. The major phytoconstituents were found to be 4H-pyran-4-one,3-hydroxy-2-methyl (9.79%), 4H-Pyran-4-one,2,3-dihydro-3,5-dihydroxy-6-methyl (6.85%), 2-furancarboxaldehyde, 5-(hydroxymethyl) (49.81%), Tetradecanoic acid (3.35%), n-Hexadecanoic acid (4.19%), Oleic Acid (6.05%), Ethyl Oleate (4.79%) and Stigmast-5-en-3-ol, (3.β.) (2.98%). Other compounds were found as minor phytoconstituents. The plant metabolites namely phytosterols, polyphenols, and

terpenoids have shown antiviral effects against several viruses [8, 32]. Based on these data, Glide Docking of SP mode was used to further examine the discovered active components in PGP extract for their virtual antiviral screening.

#### Cytotoxic analysis of pomegranate peel extract in lung cancer cell line

Lung cancer cells A549 were utilized to study the toxicity analysis of PGP extract at different doses through MTT assay. MTT assay is a colorimetric-based assay that involves the cleavage of the tetrazolium ring of MTT by Mt dehydrogenase enzymes of living cells [33]. Under inverted phase contrast microscopy, the unexposed cells remained flat, smooth, and even cell surface showing normal and healthy cells (Fig. 2A). However, pomegranate extract-exposed cells developed typical apoptotic characteristics namely nuclear condensation, substantial cytoplasmic vacuolization, and an acquired spherical shape that indicated cellular shrinkage [34]. The cell viability data showed that PGP extract resulted in a considerable decline in cell viability depending upon dose (Fig. 2B). This data suggested that PGP considerably reduced the cell viability of lung cancer cells depending upon dose. On the other hand, pomegranate extract was

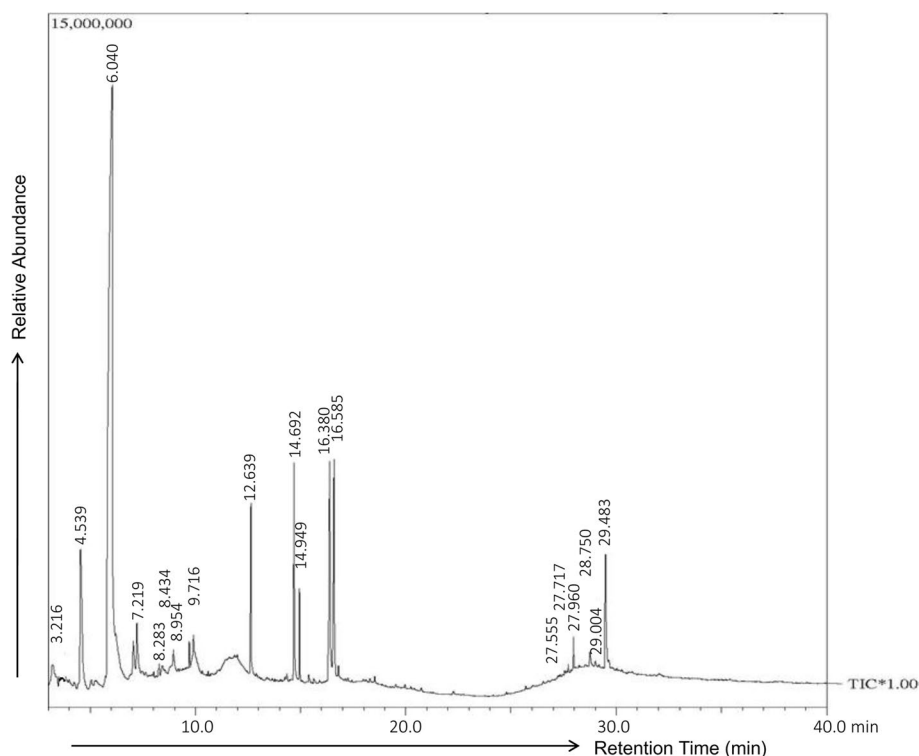


**Fig. 1** Total ion chromatogram, showing the intensities of all mass spectral peaks belonging to the same scan of the identified compounds from PGP extract (95% ethanolic)

**Table 1** The chemical constituents and their molecular formula (MF), molecular weight (MW), %Area, retention time (RT), and compound's nature from 95% ethanolic extract of PGP through GC-MS technique

S. No.	Compounds Name	Structure	PubChem CID	MF	MW	Area %	RT (min)	Nature	Fragments (m/z)
1.	1,3-Dioxolane, 2-ethenyl-2,4-dimethyl-, trans		14818495	C7H12O2	128	1.04	3.216	Heterocyclic acetal	43,27,101
2.	4H-Pyran-4-one, 2,3-dihydro-3,5-dihydroxy-6-methyl		119838	C6H8O4	144	6.85	4.539	Pyranone	43,144,101
3.	2-furancarboxaldehyde, 5-(hydroxymethyl)		237332	C6H6O3	126	49.81	6.040	Furan	97,126,41
4.	1-Amino-4-methylpiperazine		81349	C5H13N3	115	1.56	7.219	Pyridine derivative	56,99,115
5.	5H-imidazole-4-carboxylic acid, 5-amino-, ethyl ester		6424292	C6H9N3O2	155	0.34	8.283	Aromatic heterocycle imidazole (alkaloid)	155,109,127
6.	Butane, 1,1'-[methylenebis(oxy)]bis[3-methyl]		568150	C11H24O2	188	0.36	8.434	Ether	101,71,43
7.	Ethyl 5-oxo-2-pyrrolidinecarboxylate		2724446	C7H11NO3	157	0.43	8.954	Alpha-amino acid esters	84,41,157
8.	Benzoic acid, 3-ethoxy-		12126	C9H10O3	166	0.34	9.716	Carboxylic acid	138,121,166
9.	Tetradecanoic acid		11005	C14H28O2	228	3.35	12.639	Fatty acid	73,60,41
10.	n-Hexadecanoic acid		985	C16H32O2	256	4.19	14.692	Saturated fatty acid	60,73,43
11.	Hexadecanoic acid, ethyl ester		12366	C18H36O2	284	1.21	14.949	fatty acid ester	88,101,41
12.	Oleic Acid		445639	C18H34O2	282	6.05	16.380	Fatty acid	55,41,69
13.	Ethyl Oleate		5363269	C20H38O2	310	4.79	16.585	fatty acid ester	55,69,41
14.	Cholesta-4,6-dien-3-ol, (3.beta.)		14795191	C27H44O	384	0.07	27.555	Phytosterol	43,135,366
15.	Stigmast-5-en-3-ol, oleate		20831071	C47H82O2	678	0.12	27.717	Phytosterol	396,382,367,147
16.	Vitamin E		14985	C29H50O2	430	0.52	27.960	Tocopherol	165,430,43
17.	Ergost-5-en-3-ol, (3.beta.)		6428659	C28H48O	400	0.45	28.750	$\beta$ -sitosterol (phytosterol)	43,400,382,367
18.	Stigmasta-5,22-dien-3-ol		53870683	C29H48O	412	0.14	29.004	Phytosterol	55,83,412,351
19.	Stigmast-5-en-3-ol, (3.beta.)		6432744	C29H50O	414	2.98	29.483	$\beta$ -sitosterol (phytosterol)	43,81,396,414,381

tested for its intrinsic toxicity in normal kidney epithelial Vero cells. PGP extract displayed the least or no toxicity with normal cellular morphology as observed from the photomicrograph (Fig. 2C and D). Therefore, based on this result, it can be postulated that PGP extract can be used as an anticancer agent without any toxicity to normal cells.

#### Apoptosis, ROS generation and cell cycle arrest in A549 cells

Blabbing of cells, chromatic condensation, and cell shrinkage are the crucial marks of both cellular and

nuclear apoptosis. Apoptosis causes the organism's cellular balance and therefore does not cause any harm to other healthy cells [35]. Interestingly, PGP-exposed cells showed nuclear condensation, ubiquitous cytoplasmic vacuolization, and a rounded morphology indicating cellular shrinkage in comparison to the unexposed cells, the entirety of which are hallmark apoptotic characteristics. Induction of apoptosis through PGP extract depended upon dose (Fig. 3A). Further, to check whether ROS is the root cause of cell death, cells are tested for ROS generation through a fluorescence microscope and quantitatively using

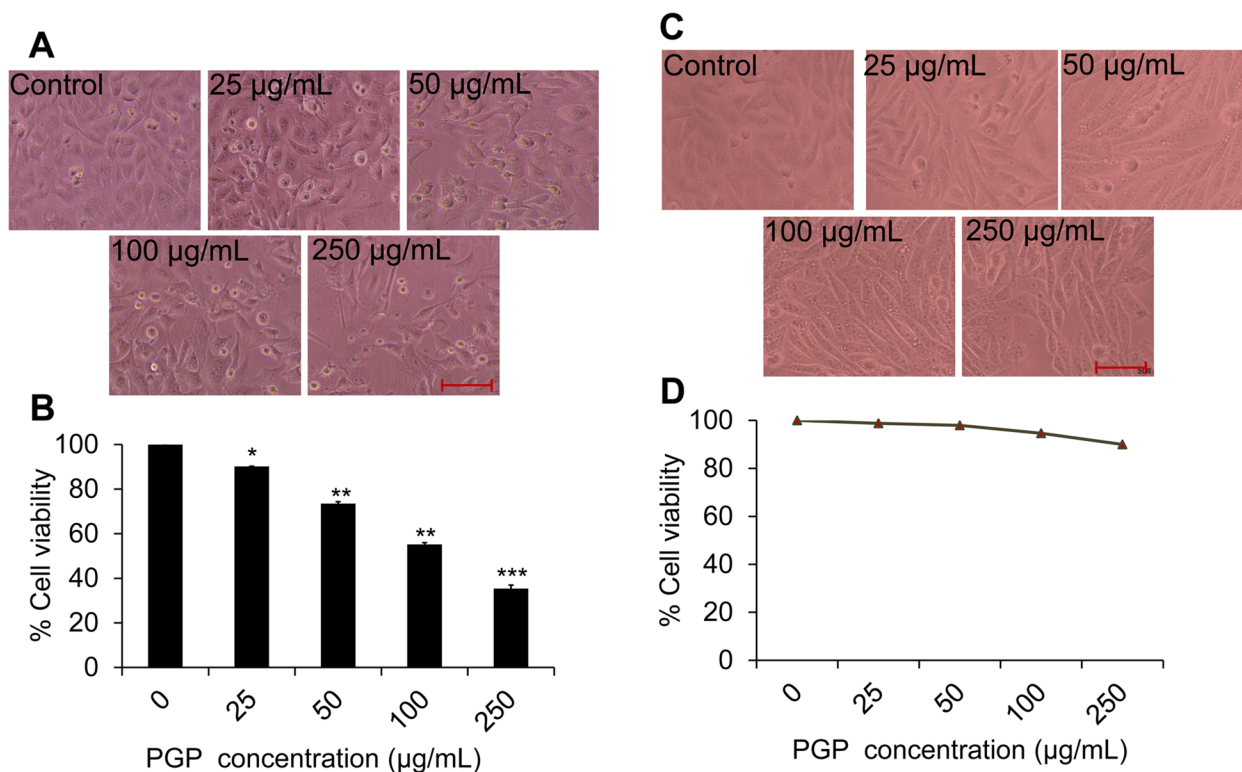


**Fig. 2** In vitro cytotoxicity test of PGP extract (25 to 250 µg/ml) in human lung cancer and normal cells **(A)** Photomicrograph of untreated and treated A549 cell line. **B** Dose–response effects of PGP extract at different concentrations on cytotoxicity in A549 cells for 24 h **(C)** Photomicrograph of untreated and treated normal Vero cell line. **D** Dose–response effects of PGP extract at different concentrations on cytotoxicity in Vero cells for 24 h. Photomicrographs were taken with an inverted phase contrast microscope. Values are expressed as means  $\pm$  SD of at least three independent experiments, \* $p < 0.05$ , \*\* $p < 0.01$  and \*\*\* $p < 0.001$  as compared to the control

a multi-plate reader. As shown in Fig. 3B and C, PGP extract induces ROS liberation by 131.13 and 196.33% respectively, when compared to control data. Additionally, ROS dynamically modifies the tumor micro-environment and is crucial in determining whether apoptosis or metastasis occurs [36]. Another factor that limits cellular growth is cell cycle arrest, and if cell division is prevented, cells die through apoptosis [37]. Figure 3D and E demonstrate that PGP extract arrested the A549 cells approx. 51.6 and 58.54% at 50 and 100 µg/ml dose, respectively as compared to control (45.5%). The present study showed that PGP extract arrested the cell cycle in  $G_0/G_1$  phase of the cell cycle.

#### Docking analysis of PGP phytocomponents

All phytocomponents from the PGP extract were tested for their ability to bind to M-pro and PL-pro proteins of COVID-19 virus using glide docking of Schrödinger maestro v2020-2. Tables 2 and 3 enlisted the details of docking score, glide score, and glide energy, Gibbs binding free energy of each component of PGP with their corresponding Mpro and PLpro proteins, respectively.

Table 2 shows that only ten phytocomponents and the standard HCQ had high binding interaction (docking score  $> -1.0$  kcal/mol) targeting the SARS-major CoV-2's protease (Mpro) protein. Comparatively, only three molecules hexadecanoic acid, ethyl ester and n-hexadecanoic acid have a weak binding interaction (docking score  $< -1.00$  kcal/mol). While other compounds did not demonstrate negative binding affinity which showed that they have no or little affinity against the targeted protein (Table S1). Stronger binding interaction between biomolecules and their proteins is indicated by the docking score's more negative values, which mimic binding free energy [38]. Following was shown to be the decreasing order of docking score of PGP phyto-constituents with Mpro protein of SARS-CoV-2: vitamin E  $>$  stigmasta-5,22-dien-3-ol  $>$  cholesta-4,6- dien-3-ol, (3. beta.)  $>$  1-Amino- 4-methylpiperazine  $>$  5- amino-5H-imidazole-4- carboxylic acid, ethyl ester  $>$  ethyl oleate  $>$  oleic Acid. Only eight phytocomponents had a negative docking score greater than  $-1.0$  kcal/mol. Molecule ethyl 5- oxo-2-pyrrolidinecarboxylate showed the best docking score ( $-5.58$  kcal/mol) in all tested compounds. The

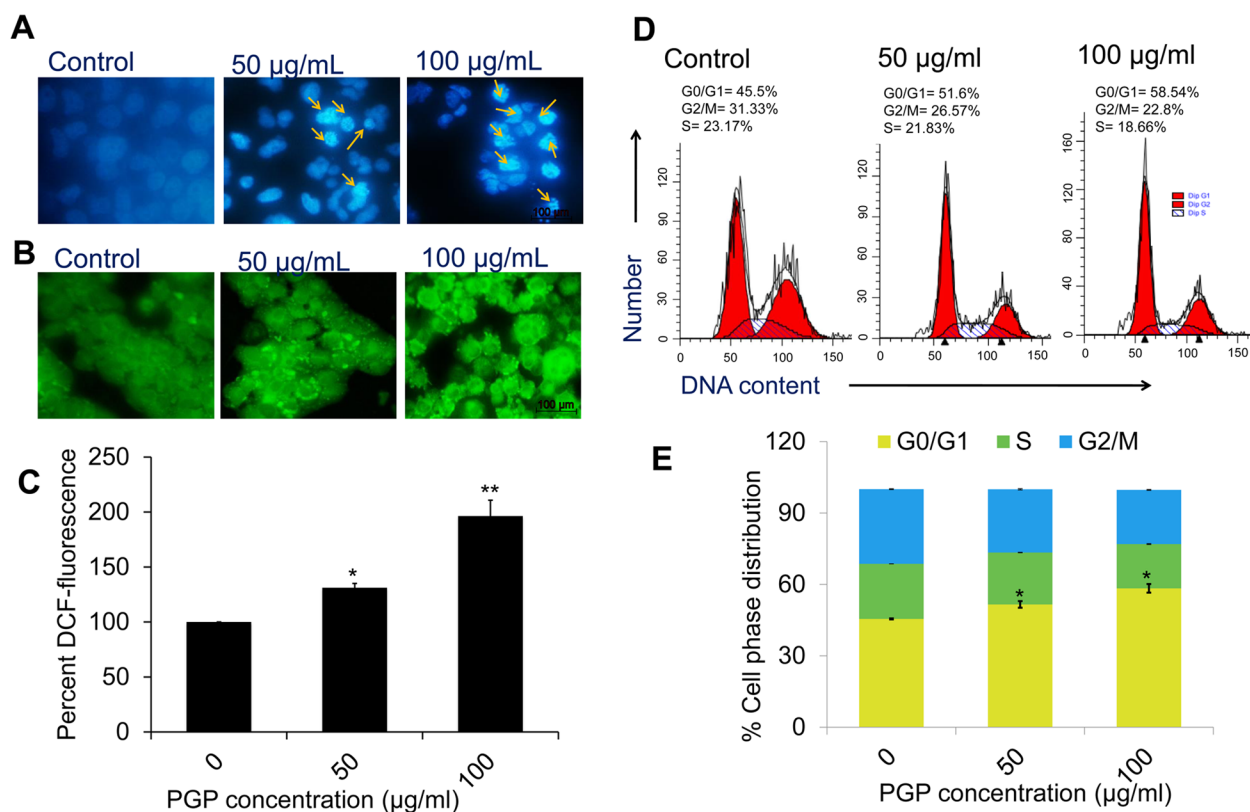


**Fig. 3** In vitro anticancer activity of PGP extract in human lung cancer A549 cells **(A)** Treated and untreated cells stained with DAPI dye were photographed under a fluorescence phase contrast microscope **(B)** Photomicrographs showed intracellular ROS production induced by PGP treatment under a fluorescence phase-contrast microscope **(C)** The percentage of fluorescence intensity relative to the control expressed by the numerical data **(D)** The Pictorial graphs show the phase distribution of cell population in A549 cells **(E)** Quantification of cell cycle phase distribution data. Cells were treated at two effective doses of PGP for 24 h, stained with propidium iodide, and measured by flow cytometry. Values are expressed as means  $\pm$  SD of at least three independent experiments, \* $p < 0.05$  and \*\* $p < 0.01$  as compared to control

non-covalent interactions *i.e.* van der Waals forces, hydrophobic and electrostatic interaction, are typically involved to bind the two molecules together in ligand–protein complexes [39]. As compounds become more lipophilic, the impact of protein binding is increased due to the hydrophobic interactions. However, as is shown in Tables 2 and 3, a variety of polar and nonpolar phyto-components' interactions with certain proteins show that a vast array of hydrophilic substances are also electrostatically bonded to protein molecules through hydrogen bonds or ionic interactions. Table 3 shows that only six PGP constituents have good binding affinities with PLpro protein in a variety of binding configurations (docking score  $> -1.0$  kcal/mol). Other compounds of PGP extract did not show binding affinity (Table S1), indicating that these substances had little to no affinity for the PLpro target protein. The standard drug HCQ had a higher binding affinity (docking score =  $-3.831$  kcal/mol) to the SARS-CoV-2 Mpro and PLpro proteins, making it an effective inhibitor. Table 3 shows that the docking score of PGP

phytochemicals with SARS-CoV-2 PLpro decreased in the following order: Cholesta- 4,6-dien-3- ol, (3.β.) > Ethyl Oleate > Stigmasta- 5,22-dien- 3-ol > Ethyl 5-oxo-2-pyrrolidinedicarboxylate > 1-Amino-4-methyl-piperazine > 5H- imidazole- 4-carboxylic acid, 5-amino-,ethyl ester. Due to electrostatic and hydrogen interactions formed between the hydroxyl groups of the molecules and various amino acid residues, only six hits (shown in Table 3) had a good docking score  $> -1.0$  kcal/mol. The top ten hits with Mpro protein and the top six hits with PLpro protein of the SARS-CoV-2 might potentially be employed to produce antiviral medicines, according to the results of Tables 2 and 3. Figure 4A depicts the 2-D LigPlot interaction between the amino acid residues Met165, His164, His41, Arg188, Tyr54, Met149, Pro52, Asp187, Gln189 of the best ligand–protein docked complex between SARS-CoV-2 Mpro and ethyl 5- oxo-2- pyrrolidinedicarboxylate. The N-group of ligand molecule is linked through one H-bond with a bond length 3.18 Å with O- group of Gln189 amino acid

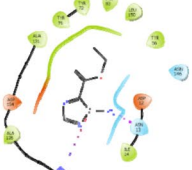
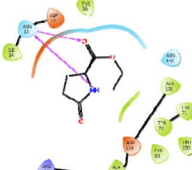
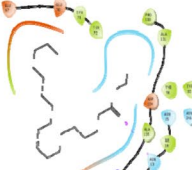
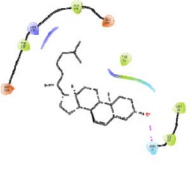
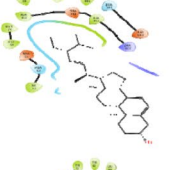
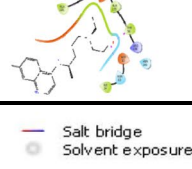
**Table 2** Various enlisted properties and 2-D interaction of the docked complex of nineteen PGP phytocomponents as well as reference drug with SARS-CoV-2 main protease (Mpro; PDB ID: 6LU7) through glide SP module (Schrödinger Maestro 2020-2)

S. No.	Ligands	Docking score (kcal/mol)	Glide E model (kcal/mol)	Glide energy (kcal/mol)	Gibbs free energy (kcal/mol)	Interacted amino acid	2-D structure of ligand-protein interaction
1.	1-Amino-4-methylpiperazine	-4.295	-26.057	-17.614	13.644	Asp187, Arg188, Gln189, Tyr54, Pro52, Met49, Cys44, His41, Met165, His164, Cys145	
2.	5H-imidazole-4-carboxylic acid, 5-amino-, ethyl ester	-4.182	-26.525	-20.264	4.205	Cys44, His41, Tyr54, Pro52, Met49, Cys145, Gly143, Asn142, Phe181, His164, Met165, Glu166, Asp187, Arg188, Gln189	
3.	Ethyl 5-oxo-2-pyrrolidine carboxylate	<b>-5.581</b>	-36.243	-28.066	1.858	Met49, Pro52, Tyr54, His41, Cys44, Asp187, Arg188, Gln189, Thr190, Gln192, His164, Met165, Glu166, Leu167, Pro168	
4.	n-Hexadecanoic acid	-0.229	-28.119	-29.417	9.373	Cys145, Ser144, Gly143, Asn142, Leu141, Met49, His163, His164, Met165, Glu166, Leu167, Pro168, His41, Asp187, Arg188, Gln189, Thr190, Ala191, Gln192	
5.	Hexadecanoic acid, ethyl ester	-0.948	-32.213	-33.887	8.369	Gln192, Ala191, Thr190, Gln189, Arg188, Asp187, Met49, Pro168, Leu167, Glu166, Met165, His164, His163, His41, Cys145, Ser144, Gly143, Asn142, Leu141, Phe140	
6.	Oleic Acid	-1.083	-31.106	-32.902	2.678	Pro168, Leu167, Glu166, Met165, His164, Gln192, Ala191, Thr190, Gln189, Arg188, Asp187, Val186, Met49, Tyr54, His41, Val42, Thr25, Thr26, Leu27, Cys145, Gly143, Asn142	
7.	Ethyl Oleate	-2.98	-36.191	-32.926	4.312	His41, Cys44, Met49, Pro52, Tyr54, Asp187, Arg188, Gln189, Thr190, Ala191, Gln192, His163, His164, Met165, Glu166, Leu167, Pro168, Cys145, Asn142	
8.	Cholesterol, (3.beta.)	-4.389	-38.555	-32.798	43.543	Tyr54, Phe181, Gln189, Arg188, Asp187, Met49, His41, Cys145, Gly143, Asn142, Leu141, His164, Met165, Glu166, Leu167, Pro168, Thr25	
9.	Vitamin E	-4.878	-47.87	-39.332	28.533	Met49, Pro52, Tyr54, His163, His164, Met165, His41, Glu166, Leu167, Pro168, Thr25, Leu27, Cys145, Ser144, Gly143, Asn142, Leu141, Phe140, Asp187, Arg188, Gln189, Thr190, Ala191, Gln192	
10.	Stigmastan-5,22-dien-3-ol	-4.736	-39.339	-31.33	42.124	His41, Cys44, Met49, Pro52, Tyr54, Cys145, Ser144, Gly143, Asn142, Leu141, Phe140, His172, Glu166, Met165, His164, His163, Phe181, Asp187, Arg188, Gln189	
11.	Hydroxychloroquine	-4.945	-52.356	-37.902	43.526	His41, His163, His164, Met165, Glu166, Phe140, Leu141, Asn142, Ser144, His172, Gln192, Thr190, Gln189, Arg188, Asp187	

Note:

- Charged (negative)
- Charged (positive)
- Glycine
- Hydrophobic
- Metal
- Polar
- Unspecified residue
- Water
- Hydration site
- Hydration site (displaced)
- Distance
- H-bond (backbone)
- H-bond (sidechain)
- Metal coordination
- Pi-Pi stacking
- Salt bridge
- Solvent exposure

**Table 3** Various enlisted properties and 2-D interaction of the docked complex of nineteen PGP phytocomponents as well as reference drug with SARS-CoV-2 papain-like protease (PLpro; PDB ID: 6W9C) through glide SP module (Schrödinger Maestro 2020-2)

S.No.	Ligands	Docking score (kcal/mol)	Glide E model (kcal/mol)	Glide energy (kcal/mol)	Gibbs binding free energy (kcal/mol)	Interacted amino acid	2-D structure of ligand-protein interaction
1.	1-Amino-4-methylpiperazine	-3.838	-22.818	-16.642	10.485	Leu150, Ala131, Asp134, Ala135, Arg138, Asn146, Tyr83, Tyr71, Asp12, Asn13, Ile14, Tyr56	
2.	5H-imidazole-4-carboxylic acid, 5-amino-, ethyl ester	-3.438	-25.639	-20.645	4.205	Tyr83, Leu150, Tyr56, Asn146, Tyr72, Tyr71, Ala131, Asp134, Ala135, Arg138, Ile14, Asn13, Asp12, Asn146	
3.	Ethyl 5-oxo-2-pyrrolidinecarboxylate	<b>-4.876</b>	-33.788	-26.398	1.858	Tyr56, Asp12, Asn13, Ile14, Asn146, Ala131, Asp134, Ala135, Arg138, Tyr71, Tyr72, Tyr83, Leu150	
4.	Ethyl Oleate	-2.306	-30.518	-30.454	4.312	Glu67, Glu70, Tyr71, Tyr72, Pro130, Ala131, Asp134, Ala135, Arg138, Tyr56, Tyr83, Leu150, Asn146, Asn15, Asn13, Asp12	
5.	Cholesterol, (3.beta.)	-2.776	-21.77	-21.489	43.543	Asp134, Tyr137, Arg138, Ala141, Glu143, Tyr71, Leu16, Ile14, Asn13	
6.	Stigmast-5,22-dien-3-ol	-1.829	-19.564	-19.019	38.342		
7.	Hydroxychloroquine	-3.831	-40.08	-33.231	41.643		

**Note:**

	Charged (negative)		Polar		Distance		Salt bridge
	Charged (positive)		Unspecified residue		H-bond (backbone)		Solvent exposure
	Glycine		Water		H-bond (sidechain)		
	Hydrophobic		Hydration site		Metal coordination		
	Metal		Hydration site (displaced)		Pi-Pi stacking		

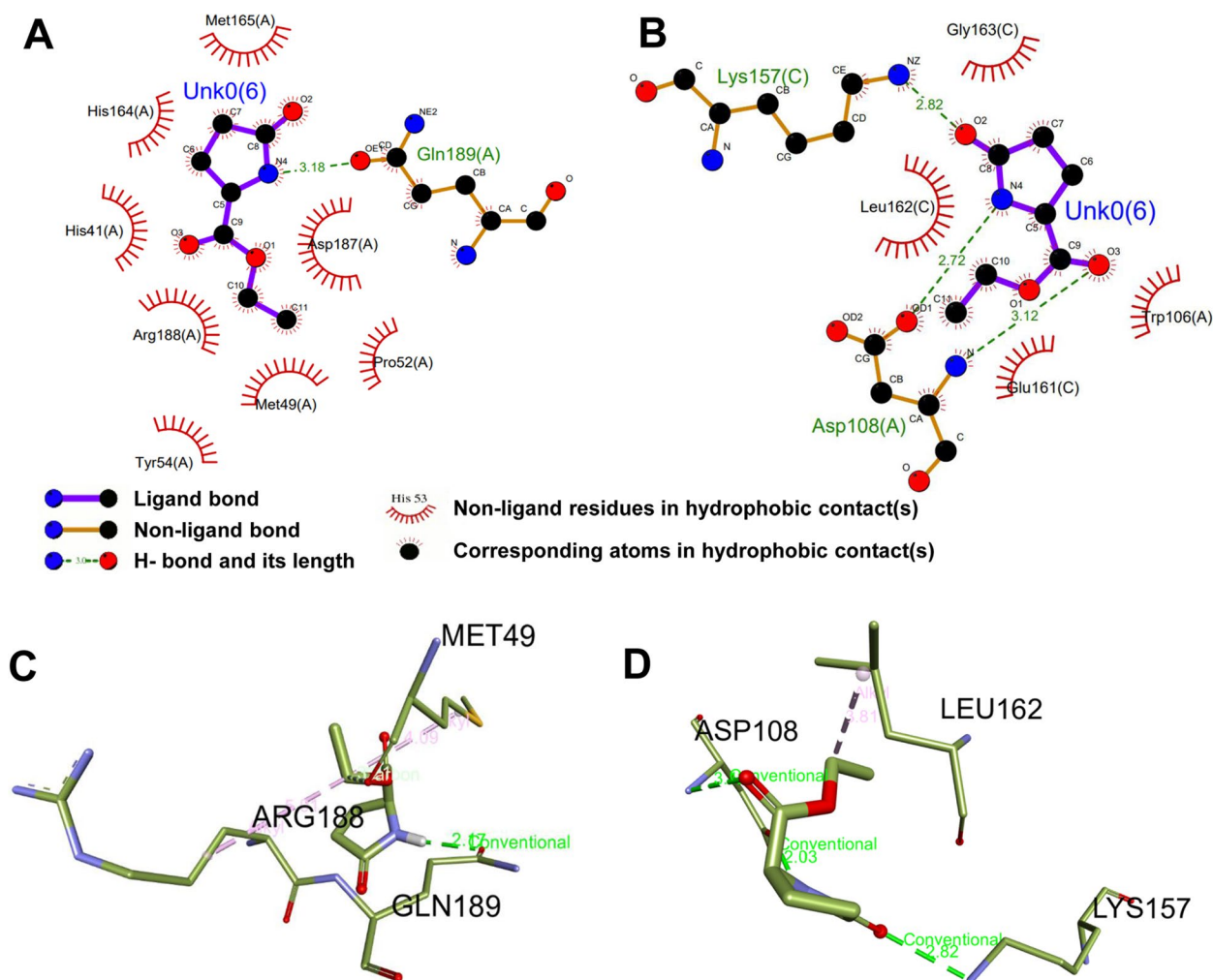


**Fig. 4** **A** Interaction between a best-docked complex of ethyl 5-oxo-2-pyrrolidinecarboxylate and SARS-CoV-2 main protease (Mpro; PDB ID: 6LU7) using Ligplot. Only one residue (Gln189, H-bond = 3.18 Å) of protein was involved in the hydrogen bond between the O-group of protein and the N-group of ligand **(B)** Interaction between the best-docked complex of ethyl 5-oxo-2-pyrrolidinecarboxylate and SARS-CoV-2 papain-like protease (PLpro; PDB ID: 6W9C) using Ligplot. Three H-bonds are involved in the docked complex: i) between N-group of amino acid residue and O-group of ligand with bond length 2.82 Å, ii) between O-group of amino acid residue and N-group of ligand with bond length 2.72 Å, and iii) between N-group of amino acid residue and O-group of ligand with bond length 3.12 Å. The red-brown color in the half-circle indicates the residue of proteins that are involved in hydrophobic interaction with ligands. Green dotted lines show the hydrogen bond and the value indicates their bond length. **C** and **D** represents 3-D interaction by Ball and Stick model of interacting amino acids residues of SARS-CoV-2 Mpro and PLpro with ethyl 5-oxo-2-pyrrolidinecarboxylate, respectively using BIOVIA Discovery Studio 2021

residue of the protein. While other amino acid residues are linked with hydrophobic interaction with ligand. Figure 4B represents the 2-D LigPlot interaction between the amino acid residues Gly163, Lys157, Leu162, Asp108, Glu161, and Trp106 of the best ligand–protein docked complex between PLpro and ethyl 5-oxo-2-pyrrolidinecarboxylate. The O-group of ligand molecule is linked through three H-bonds with three different amino acid residues of proteins e.g. 1) O-group of ligand molecule

is linked through one H-bond with Lys157 residues of proteins with a bond length 2.82 Å, 2) N-group of ligand molecule is linked through one H-bond with O-group of Asp108 residues of proteins with a bond length 2.72 Å, and 3) O- group of ligand molecule is linked through one H-bond with N-group of Asp108 amino acid residue of the protein. Gly163, Leu162, Glu161, and Trp106 amino acid residues are interacted with hydrophobic bonds. Figure 4C and D show the 3-D interaction of amino acid

residues of SARS-CoV-2 Mpro and PLpro with ethyl 5-oxo-2-pyrrolidinecarboxylate, respectively using BIOVIA Discovery Studio 2021.

Phytochemicals of different classes including pyridine, imidazole, alpha amino acid esters, fatty acid ester, tocopherol, and phytosterol and their derivatives were detected as chief components in PGP extract and, these compounds showed strong affinity towards Mpro and PLpro proteins (Tables 1, 2 and 3). Pyridine is a preferred heterocycle nucleus, and its compounds have been studied for their medicinal effects, including those against pathogens, viruses, tumors, analgesics, convulsants, inflammation, antioxidants, Alzheimer's, ulcers, and diabetes [40]. Imidazole, an aromatic heterocycle, classified as a diazole, has been effectively used in the treatment of several life-threatening and infectious diseases. It displays a wide range of biological activities, including antiviral, anticancer, anti-diabetic, antibacterial, antifungal, and anti-inflammatory [41]. Amino acid esters are extensible chiral auxiliary groups that are used in the asymmetric synthesis of pharmaceutically important nitrogen heterocycles. Amino acid esters are helpful in the development of prodrugs as anticancer and antiviral drugs because they have a higher bioavailability and lower toxicity, deliver the medication precisely to the target tissues or organs, and slow down the metabolism [42]. In a previous study, fatty acids profile and heterocyclic derivatives of green seaweeds have shown greater anticancer potentials rather than green seaweed-based food [43]. A previous report has described the anticancer potential of saturated/unsaturated fatty acids and heterocyclic compounds against various tumor cells namely colorectal cancer (Caco-2, HT-29), breast cancer (MCF-7, MDA-MB-231), skin epidermoid (A431), prostate cancer (PC-3), human cervical carcinoma cell lines (KB-3-1), human neuroblastoma cells (GOTO, NCG), etc. [44]. Tocopherols, which are phenolic antioxidants, work with singlet oxygen to scavenge free radicals and stop lipid oxidation [45]. A previous study showed that viral and retroviral reproduction were suppressed by providing the formulation containing vitamin E, tocopherol, or tocopherol derivative [46]. Alpha-tocopherol can interact with RNA-dependent RNA polymerase of SARS-CoV-2 through solubilizing modifications, making it a potent antiviral drug alone and even more so in combination with remdesivir [47]. Similar to cholesterol, phytosterols are phytosteroids that plants employ as building blocks for their biological membranes. The phytosterol present in the bark of *Picea abies* has been shown to have antioxidant, antibacterial, and antifungal qualities [48]. Monoterpenes and their derivatives namely emodin, carvacrol, thymol and artemisinin exhibited strong binding affinity with

spike glycoproteins of SARS-CoV-2 and ACE2 receptor predicting the prevention of SARS-CoV-2 interaction with ACE-2 receptor in COVID 19 pathogenesis [49]. Moreover, the anthraquinones and their derivatives viz. anthrarrufin, alizarine, emodin, aloe-emodin, and dantron have shown good binding affinity with the RNA binding domain of nucleocapsid phosphoprotein of COVID-19, preventing virus assembly for propagation [50]. These earlier studies and the most recent in silico analysis suggest that natural compounds found in PGP may be used as therapeutic candidates.

### MD simulation study

To evaluate the accuracy of a simulation and the stability of a ligand–protein complex structure over time, the RMSD is determined [51]. The ligand–protein complex's stable interaction was shown by the RMSD analysis of the ethyl 5-oxo-2-pyrrolidinecarboxylate-PLpro and Mpro complexes, which were performed using a protein and ligand fit on protein backbone (Fig. 5A and B). Table 4 and Fig. 5A demonstrate that the RMSD of the Mpro backbone ranged from 0.0004952–0.3934001 nm, whereas the RMSD of the ethyl 5-oxo-2-pyrrolidinecarboxylate lig-fit on protein was between 0.0005589 and 8.093586 nm. The ethyl 5-oxo-2-pyrrolidinecarboxylate lig-fit on protein RMSD ranged between 0.000557–11.5442219 nm, whereas the protein backbone RMSD ranged between 0.0005053–5.6615124 nm (Table 4, Fig. 5B). The RMSD value of PLpro was found to be much more stable. The protein's backbone trajectory's secondary structural variation is determined using the RMSF analysis [52]. The backbones of the Mpro-ligand and PLpro-ligand complexes had RMSF values ranging from 0.0433–1.0568 and 1.4328–6.1267 nm, respectively (Table 4, Fig. 5A and B). The range of the ligand's Rg with both proteins was found to be 0.23114–0.27668 nm and 0.229083–0.272896 nm, respectively. The number of H-bonds between ligand and protein was counted throughout each simulation frame [53]. A maximum of four H-bonds were present in the ethyl 5-oxo-2-pyrrolidinecarboxylate-Mpro complex throughout 100 ns MD simulation (Fig. 2A). Whereas ethyl 5-oxo-2-pyrrolidinecarboxylate-PLpro complex maximum displayed 6 H-bonds and for the majority of the time frame it maintained 4 H-bond throughout 100 ns MD simulation (Fig. 3D). This allowed for a noticeably more stable configuration. SASA provides a crucial explanation of ligand binding. The amount of the ligand SASA value reduction indicates whether the ligand is thoroughly buried after binding to the pocket. The SASA value for both complexes ranged between 3.056–4.08 and 3.106–4.155 nm<sup>2</sup>, respectively (Table 4, Fig. 2A and B). The change in free energy is a very important physical

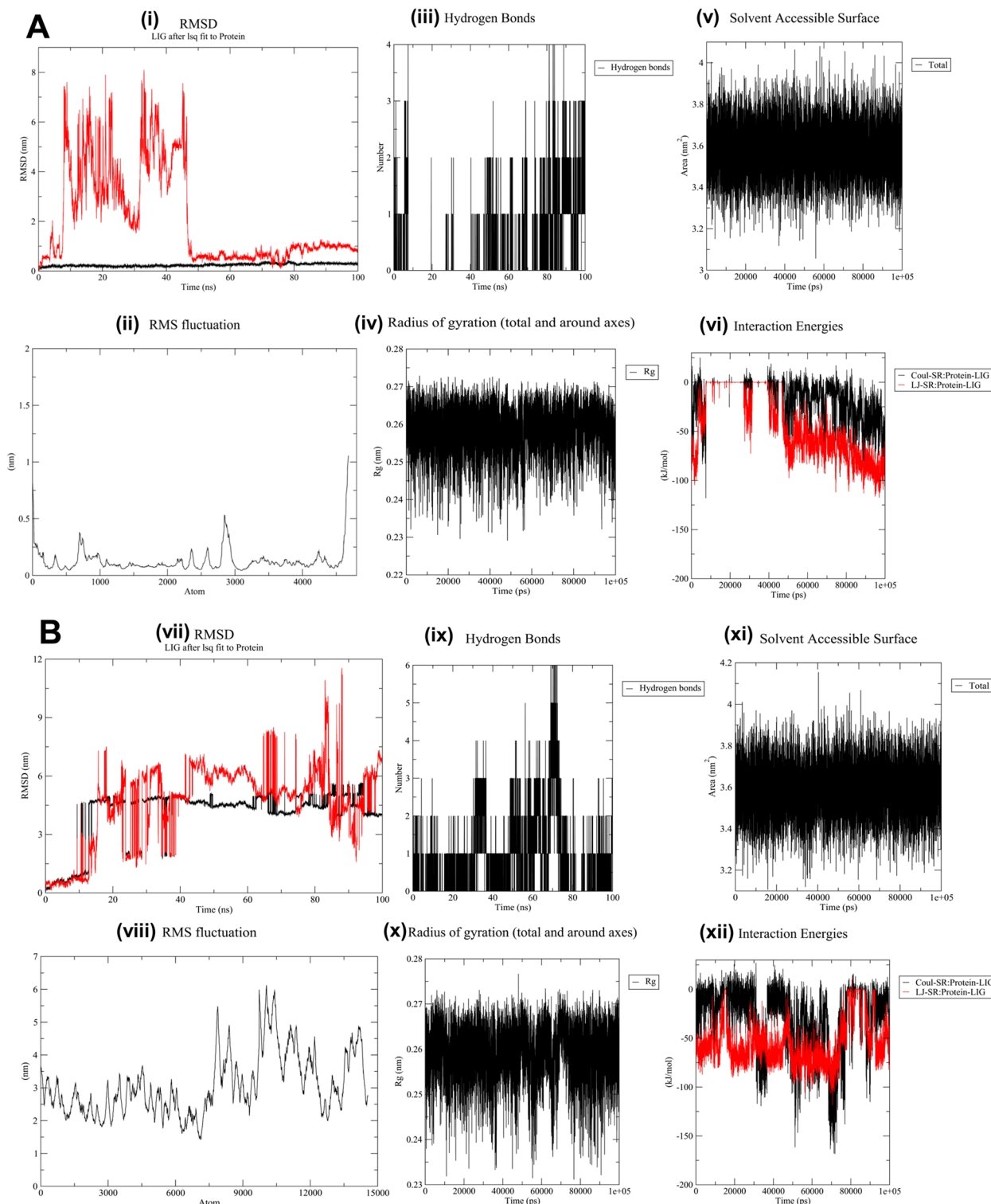


**Fig. 5** MD simulation trajectory of **(A)** ethyl 5-oxo-2-pyrrolidinecarboxylate- Mpro and **(B)** ethyl 5-oxo-2-pyrrolidinecarboxylate- PLpro complex at 100 ns. (i, vii) RMSD value of Mpro and PLpro unbound (black) with ligand (Red), respectively. (ii, viii) RMSF value of Mpro and PLpro backbone residue, respectively (iii, ix) Plot of hydrogen bond of the ligand–protein complex. (iv, x) Rg of ligand (v, xi) SASA of both complex (vi, xii) Interaction energy of both complex

**Table 4** MD simulation properties of Ethyl 5-oxo-2-pyrrolidinecarboxylate- Mpro complex and Ethyl 5-oxo-2-pyrrolidinecarboxylate-PLpro complex

S. No	MD simulation properties	Ethyl 5-oxo-2-pyrrolidinecarboxylate-Mpro complex	Ethyl 5-oxo-2-pyrrolidinecarboxylate-PLpro complex
1	RMSD protein Backbone (nm)	0.0004952–0.3934001	0.0005053–5.6615124
2	RMSD lig-fit on protein (nm)	0.0005589–8.093586	0.000557–11.5442219
3	RMSF protein Backbone (nm)	0.0433–1.0568	1.4328–6.1267
4	Radius of gyration (nm)	0.229083–0.272896	0.23114–0.27668
5	Solvent Accessible Surface (nm <sup>2</sup> )	3.056–4.08	3.106–4.155
6	Coul-SR: Protein-LIG (kJ/mol)	-15.46 ± 20.11	-29.50 ± 33.25
7	LJ-SR:Protein-LIG (kJ/mol)	-44.13 ± 34.09	-55.96 ± 22.79
8	Total interaction energy (kJ/mol)	-59.59 ± 27.07	-85.46 ± 28.02

component that affects many biological processes [54]. The short-range Lennard–Jones energy (LJ-SR) and Coulombic energy (Coul-SR) were used to extract the interaction energy between ligands and proteins. For the ethyl 5-oxo-2-pyrrolidinecarboxylate-Mpro complex, the average Coul-SR interaction energy was  $-15.46 \pm 20.11$  kJ/mol; the LJ-SR energy was determined to be  $-44.13 \pm 34.09$  kJ/mol and the total interaction energy was measured to be  $-59.59 \pm 27.07$ . The average Coul-SR interaction energy and LJ-SR energy of the ethyl 5-oxo-2-pyrrolidinecarboxylate-PLpro complex were  $-29.50 \pm 33.25$  kJ/mol and  $-55.96 \pm 22.79$  kJ/mol, respectively. The total interaction energy of this complex was determined to be  $-85.46 \pm 28.02$  kJ/mol (Table 4, Fig. 4A and B).

#### Toxicity profile and physicochemical properties

Table 4 displays the physicochemical characteristics of PGP phytoconstituents. For an orally active drug, Lipinski should have no or only one violation [55]. Four phytoconstituents showed no violations while the remaining four components of PGP showed only one violation of Lipinski's rule of five. HCQ, on the other hand, showed no violation. The oral absorption rate, or the percentage of pharmaceuticals that pass through the portal vein and into the bloodstream from the gastrointestinal lumen, is represented by the percentage of medications that are absorbed [56]. The results of activity spectra for drugs show that more than >50% of the medicine is available in the gastrointestinal lumen (Table 1; Column 3). TPSA can be used as a useful molecular descriptor in the research of drug transport qualities including blood–brain barrier (BBB) penetration and intestinal absorption. Additionally, it is a good indicator of how well-absorbed pharmaceuticals will be by

cells. TPSA contributes to a molecule's surface area—typically van der Waals—namely oxygen, nitrogen, and their accompanying hydrogen atoms [57]. Molecules with polar surface areas over 160 Å are frequently hard to get through cell membranes. Interestingly, Table 4 shows that all phytoconstituents had TPSA values less than 160 Å, indicating sufficient absorption through the intestinal wall. The toxicity potential and drug-likeness of PGP phytoconstituents are shown in Tables 5 and 6. The findings showed that, except for a few values, all phytoconstituents are found to be safe without any known mutagenic, tumorigenic, harmful effects on reproduction, or irritant properties. The current computational analysis of PGP constituents revealed many benefits and drawbacks for distinct parts; nonetheless, the majority of the phytoconstituents exhibited potent antiviral activity and drug-like characteristics.

#### Conclusions

In conclusion, phytochemical analyzed by GC–MS technique showed nineteen phytoconstituents of different groups namely pyridine, imidazole, alpha amino acid esters, polyphenols, fatty acid ester, aliphatic hydrocarbons, tocopherol and phytosterol, and their derivatives. The top ten hits of PGP phyto-active components showed a potent binding affinity with Mpro and the top six hits with PLpro protein of SARS-CoV-2. Throughout a 100 ns simulation, the best-docked complex, ethyl 5-oxo-2-pyrrolidinecarboxylate, with PLpro and Mpro proteins, exhibited almost stable interaction. Interestingly, most of the phytoconstituents displayed orally active drug with and drug-likeness with no non-tumorigenic activity. In addition, PGP inhibits the human lung cancer A549 cells without any

**Table 5** PASS analysis of lead molecules of PGP extract

Lipinski's rule of 5 (Physicochemical Properties)										
S.No	Phytoconstituents	% Absorption <sup>a</sup> (> 50%)	Topological Polar Surface Area (Å) <sup>2</sup> (TPSA) <sup>b</sup> (< 160 Å)	MW (< 500)	c logP <sup>c</sup> (< 5)	Heavy atom count (n atom)	Hydrogen Bond Donors (nOHNH) (≤ 5)	Hydrogen Bond Acceptors (nON) (≤ 10)	Number of Rotatable bonds (≤ 10)	Lipinski's violation
1	1-Amino-4-methylpiperazine	97.78	32.50	115.18	-0.38	8	2	3	0	0
2	5H-imidazole-4-carboxylic acid, 5-amino-, ethyl ester	82.41	77.06	155.16		11	2	5	3	0
3	Ethyl 5-oxo-2-pyrrolidinecarboxylate	89.88	55.40	157.17	0.05	11	1	4	3	0
4	Oleic Acid	96.13	37.30	282.47	7.58	15	1	2	15	1
5	Ethyl Oleate	99.92	26.30	310.52	8.24	22	0	2	17	1
6	Cholesta-4,6-dien-3-ol, (3.beta.)	102.02	20.23	384.65	7.11	28	1	1	5	1
7	Vitamin E	98.83	29.46	430.72	9.04	31	1	2	12	1
8	Stigmasta-5,22-dien-3-ol	102.02	20.23	412.70	7.87	30	1	1	5	0
9	Hydroxychloroquine	92.302	48.4	335.9	3.08	23	2	4	9	0

<sup>a</sup> Percentage absorption was calculated as: % Absorption = 109 - [0.345x Topological Polar Surface Area]

<sup>b</sup> Topological polar surface area (defined as a sum of surfaces of polar atoms in a molecule)

<sup>c</sup> Logarithm of compound partition coefficient between n-octanol and water

**Table 6** Druglikeness and toxicity calculation of lead molecules of PGP extract

S. No	Compounds Name	Drug-likeness	Mutant	Tumorigenic	Reproductive effective	Irritant
1	1-Amino-4-methylpiperazine	3.9861	H	H	N	N
2	5H-imidazole-4-carboxylic acid, 5-amino-, ethyl ester	-2.5139	N	N	N	N
3	Ethyl 5-oxo-2-pyrrolidinecarboxylate	-0.4895	N	N	N	N
4	Oleic Acid	-28.971	H	H	N	H
5	Ethyl Oleate	-43.109	N	N	N	N
6	Cholesta-4,6-dien-3-ol, (3.β.)	-2.3126	N	N	H	H
7	Vitamin E	-3.2757	N	N	N	N
8	Stigmasta-5,22-dien-3-ol	1.2217	N	N	N	N
9	Hydroxychloroquine	5.73	H	N	N	N

N- No toxicity

L- Low toxicity

H- High toxicity

known toxicity to normal cells. The leading cause of cell death was the stimulation of ROS by PGP extract, which caused cell cycle arrest and ultimately apoptosis. The finding of the study suggests that pomegranate peel could act as a dual agent targeting lung cancer cell death as well as COVID-19 pathogenesis, however, additional research is required to confirm their effects.

#### Abbreviations

COVID-19	Coronavirus ailment 2019
DAPI	4, 6-Diamidino-2 Phenylindole
GC-MS	Gas chromatography-mass spectroscopy
Mpro	Main protease
MTT	3-(4,5-Dimethylthiazol-2-yl)-2,5-Diphenyltetrazolium Bromide
PGP	<i>Punica granatum</i> Peel
PLpro	Papain-like protease
ROS	Reactive oxygen species
SARS-CoV-2	Severe acute respiratory syndrome coronavirus 2
SP	Standard precision

#### Supplementary Information

The online version contains supplementary material available at <https://doi.org/10.1186/s12906-024-04738-1>.

- Supplementary Material 1.

Supplementary Material 2.

#### Acknowledgements

The authors extend their appreciation to the Deanship of Research and Graduate Studies at King Khalid University for funding the work through Small Research Group under grant number RGP1/74/45. The authors express their sincere thanks to the Central Instrumentation Facility, Era University and University of Lucknow, India.

#### Authors' contributions

M.A.B, T.A. and S.S. conceptualization, designed, and performed the experiment. M.A.B, M.Z.H. and S.S. wrote the main manuscript. M.A.B., A.F., B. R., M.Z.H., T.A, H.B. and S.S. analyzed the data and interpreted the results. A.A.A., H.B., A.F.A and Y.I.A provided the critical inputs and edited the manuscript. All authors reviewed the manuscript.

#### Funding

The authors extend their appreciation to the Deanship of Research and Graduate Studies at King Khalid University for funding the work through Small Research Group under grant number RGP1/74/45.

#### Data availability

The datasets used and analyzed in the current study are included in this article.

#### Declarations

#### Ethics approval and consent to participate

Not applicable.

#### Consent for publication

Not applicable.

#### Competing interests

The authors declare no competing interests.

#### Author details

<sup>1</sup>Department of Pharmaceutics, College of Pharmacy, University of Hafr Al-Batin, Al Jamiah, 39524 Hafr Al Batin, Saudi Arabia. <sup>2</sup>Department of Pharmacy Practice, College of Pharmacy, University of Hafr Al Batin, 39524 Hafr Al Batin, Saudi Arabia. <sup>3</sup>Department of Pharmaceutical Chemistry, College of Pharmacy, King Khalid University, Asir, Saudi Arabia. <sup>4</sup>Department of Biotechnology, Era's Lucknow Medical College and Hospital, Era University, Lucknow, India. <sup>5</sup>Department of Pharmaceutical Chemistry, College of Pharmacy, University of Hafr Al-Batin, Al Jamiah, 39524 Hafr Al Batin, Saudi Arabia. <sup>6</sup>Department of Pharmacology, College of Pharmacy, King Khalid University, Asir, Saudi Arabia.

Received: 1 November 2023 Accepted: 19 December 2024

Published online: 30 January 2025

#### References

- Lai CC, Shih TP, Ko WC, Tang HJ, Hsueh PR. Severe acute respiratory syndrome coronavirus 2 (SARS-CoV-2) and coronavirus disease-2019 (COVID-19): The epidemic and the challenges. *Int J Antimicrob Agents*. 2022;55(3):105924.
- Pathania AS, Prathipati P, Abdul BA, Chava S, Katta SS, Gupta SC, Gangula PR, Pandey MK, Durden DL, Byrareddy SN, Challagundla KB. COVID-19

- and cancer comorbidity: therapeutic opportunities and challenges. *Theranostics*. 2021;11(2):731–53. <https://doi.org/10.7150/thno.51471>. PMID: 33391502; PMCID: PMC7738845.
3. Passaro A, Bestvina C, Velez Velez M, Garassino MC, Garon E, Peters S. Severity of COVID-19 in patients with lung cancer: evidence and challenges. *J Immunother Cancer*. 2021;9(3):e002266.
  4. Tian J, Yuan X, Xiao J, Zhong Q, Yang C, Liu B, Cai Y, Lu Z, Wang J, Wang Y, Liu S. Clinical characteristics and risk factors associated with COVID-19 disease severity in patients with cancer in Wuhan, China: a multicentre, retrospective, cohort study. *Lancet Oncol*. 2020;21(7):893–903.
  5. Chugh A, Sehgal I, Khurana N, Verma K, Rolta R, Vats P, Salaria D, Fadare OA, Awofisayo O, Verma A, Phartyal R. Comparative docking studies of drugs and phytochemicals for emerging variants of SARS-CoV-2. *3 Biotech*. 2023;13(1):36.
  6. Sohrabi C, Alsafi Z, O'Neill N, Khan M, Kerwan A, Al-Jabir A, Iosifidis C, Agha R. World Health Organization declares global emergency: a review of the 2019 novel coronavirus (COVID-19). *Int J Surg*. 2020;76:71–6.
  7. Rome BN, Avorn J. Drug evaluation during the COVID-19 pandemic. *N Engl J Med*. 2020;382(24):2282–4.
  8. Behl T, Rocchetti G, Chadha S, Zengin G, Bungau S, Kumar A, Mehta V, Uddin MS, Khullar G, Setia D, Arora S. Phytochemicals from plant foods as potential source of antiviral agents: an overview. *Pharmaceuticals*. 2021;14(4):381.
  9. Huang F, Li Y, Leung EL, Liu X, Liu K, Wang Q, Lan Y, Li X, Yu H, Cui L, Luo H. A review of therapeutic agents and Chinese herbal medicines against SARS-CoV-2 (COVID-19). *Pharmacol res*. 2020;1(158): 104929.
  10. Panyod S, Ho CT, Sheen LY. Dietary therapy and herbal medicine for COVID-19 prevention: a review and perspective. *J Tradit Complement Med*. 2020;10(4):420–7.
  11. Maphetu N, Unuofin JO, Masuku NP, Olisah C, Lebelo SL. Medicinal uses, pharmacological activities, phytochemistry, and the molecular mechanisms of *Punica granatum* L. (pomegranate) plant extracts: a review. *Biomed Pharmacother*. 2022;153:113256.
  12. Pienaar L, Barends-Jones V. The economic contribution of South Africa's pomegranate industry. *Agriprobe*. 2021;18(4):57–64.
  13. Mo Y, Ma J, Gao W, Zhang L, Li J, Li J, Zhang J. Pomegranate peel as a source of bioactive compounds: a mini review on their physiological functions. *Front Nutr*. 2022;9:887113.
  14. Shaygannia E, Bahmani M, Zamanzad B, Rafieian-Kopaei M. A review study on *Punica granatum* L. *J Evid Based Complement Altern Med*. 2016;21(3):221–7.
  15. Salles TS, Meneses MDF, Caldas LA, Sá-Guimarães TE, de Oliveira DM, Ventura JA, Azevedo RC, Kuster RM, Soares MR, Ferreira DF. Virucidal and antiviral activities of pomegranate (*Punica granatum*) extract against the mosquito-borne Mayaro virus. *Parasit Vectors*. 2021;14(1):443.
  16. Neurath AR, Strick N, Li YY, Debnath AK. *Punica granatum* (pomegranate) juice provides an HIV-1 entry inhibitor and candidate topical microbicide. *Ann N Y Acad Sci*. 2005;1056:311–27.
  17. Al-Zoreky NS. Antimicrobial activity of pomegranate (*Punica granatum* L.) fruit peels. *Int J Food Microbiol*. 2009;134(3):244–8.
  18. Das S, Sarmah S, Lyndem S, Singha RA. An investigation into the identification of potential inhibitors of SARS-CoV-2 main protease using molecular docking study. *J Biomol Struct Dyn*. 2021;39(9):3347–57.
  19. Amin SA, Banerjee S, Ghosh K, Gayen S, Jha T. Protease targeted COVID-19 drug discovery and its challenges: Insight into viral main protease (Mpro) and papain-like protease (PLpro) inhibitors. *Bioorg Med Chem*. 2021;1(29):115860.
  20. Siddiqui S, Upadhyay S, Ahmad I, Hussain A, Ahamed M. Cytotoxicity of *Moringa oleifera* fruits on human liver cancer and molecular docking analysis of bioactive constituents against caspase-3 enzyme. *J Food Biochem*. 2021;45(5):e13720.
  21. Siddiqui S, Ahmad E, Gupta M, Rawat V, Shivnath N, Banerjee M, Khan MS, Arshad M. *Cissus quadrangularis* Linn exerts dose-dependent biphasic effects: osteogenic and anti-proliferative, through modulating ROS, cell cycle and Runx2 gene expression in primary rat osteoblasts. *Cell Prolif*. 2015;48(4):443–54.
  22. Kaleem S, Siddiqui S, Siddiqui HH, Badruddeen, Hussain A, Arshad M, Akhtar J, Rizvi A. Eupalitin induces apoptosis in prostate carcinoma cells through ROS generation and increase of caspase-3 activity. *Cell Biol Int*. 2016;40(2):196–203.
  23. Sahayarayan JJ, Rajan KS, Vidhyavathi R, Nachiappan M, Prabhu D, Alfarraj S, Arokiyaraj S, Daniel AN. In-silico protein-ligand docking studies against the estrogen protein of breast cancer using pharmacophore based virtual screening approaches. *Saudi J Biol Sci*. 2021;28(1):400–7.
  24. Owoloye AJ, Ligali FC, Enejoh OA, Musa AZ, Aina O, Idowu ET, Oyebola KM. Molecular docking, simulation and binding free energy analysis of small molecules as PfHT1 inhibitors. *PLoS ONE*. 2022;17(8):e0268269.
  25. Culletta G, Gulotta MR, Perricone U, Zappalà M, Almerico AM, Tutone M. Exploring the SARS-CoV-2 proteome in the search of potential inhibitors via structure-based pharmacophore modeling/docking approach. *Computation*. 2020;8(3):77.
  26. Siddique F, Anwaar A, Bashir M, Nadeem S, Rawat R, Eyupoglu V, Afzal S, Bibi M, Bin Jardan YA, Bourhia M. Revisiting methotrexate and phototretate Zinc15 library-based derivatives using deep learning *in-silico* drug design approach. *Front Chem*. 2024;21(12):1380266.
  27. Ribeiro R, Botelho FD, Pinto AMV, La Torre AMA, Almeida JSFD, LaPlante SR, Franca TCC, Veiga-Junior VF, Dos Santos MC. Molecular modeling study of natural products as potential bioactive compounds against SARS-CoV-2. *J Mol Model*. 2023;29(6):183.
  28. Lipinski CA. Lead- and drug-like compounds: the rule-of-five revolution. *Drug Discov Today Technol*. 2004;1(4):337–41.
  29. Popova M, Dimitrova R, Al-Lawati HT, Tsvetkova I, Najdenski H, Bankova V. Omani propolis: chemical profiling, antibacterial activity and new propolis plant sources. *Chem Cent J*. 2013;7(1):158.
  30. Villas-Bôas SG, Mas S, Akesson M, Smedsgaard J, Nielsen J. Mass spectrometry in metabolome analysis. *Mass Spectrom Rev*. 2005;24(5):613–46.
  31. Singh G, Lu D, Liu C, Hower D. Analytical challenges and recent advances in the identification and quantitation of extractables and leachables in pharmaceutical and medical products. *TrAC - Trends Anal Chem*. 2021;1(141):116286.
  32. El-Missiry MA, Fekri A, Kesar LA, Othman AI. Polyphenols are potential nutritional adjuvants for targeting COVID-19. *Phytother Res*. 2021;35(6):2879–89.
  33. Mosmann T. Rapid colorimetric assay for cellular growth and survival: application to proliferation and cytotoxicity assays. *J Immunol Methods*. 1983;65(1–2):55–63.
  34. Buttacavoli M, Albanese NN, Di Cara G, Alduina R, Faleri C, Gallo M, Pizzolanti G, Gallo G, Feo S, Baldi F, Cancemi P. Anticancer activity of biogenerated silver nanoparticles: an integrated proteomic investigation. *Oncotarget*. 2018;9(11):9685.
  35. Wong RS. Apoptosis in cancer: from pathogenesis to treatment. *J Exp Clin Cancer Res*. 2011;30(1):87.
  36. Aggarwal V, Tuli HS, Varol A, Thakral F, Yerer MB, Sak K, Varol M, Jain A, Khan MA, Sethi G. Role of reactive oxygen species in cancer progression: molecular mechanisms and recent advancements. *Biomolecules*. 2019;9(11):735.
  37. Kumari R, Jat P. Mechanisms of cellular senescence: cell cycle arrest and senescence associated secretory phenotype. *Front Cell Dev Biol*. 2021;29(9):645593.
  38. Friesner RA, Murphy RB, Repasky MP, Frye LL, Greenwood JR, Halgren TA, Sanschagrin PC, Mainz DT. Extra precision glide: Docking and scoring incorporating a model of hydrophobic enclosure for protein–ligand complexes. *J Med Chem*. 2006;49(21):6177–96.
  39. Du X, Li Y, Xia YL, Ai SM, Liang J, Sang P, Ji XL, Liu SQ. Insights into protein-ligand interactions: mechanisms, models, and methods. *Int J Mol Sci*. 2016;17(2):144.
  40. Marinescu M, Popa CV. Pyridine compounds with antimicrobial and antiviral activities. *Int J Mol Sci*. 2022;23(10):5659.
  41. Gupta GK, Kumar V, Kaur K. Imidazole containing natural products as antimicrobial agents: a review. *Nat Prod J*. 2014;4(2):73–81.
  42. Vale N, Ferreira A, Matos J, Fresco P, Gouveia MJ. Amino acids in the development of prodrugs. *Molecules*. 2018;23(9):2318.
  43. Taher N, Mentang F, Montolalu RI, Gunawan WB, Taslim NA, Mayulu N, Nurkolis F. Green seaweeds fatty acids and heterocyclic derivatives against cancer: Opinion on future nutraceutical application. *Front Oncol*. 2023;14(13):1145919.
  44. Józwiak M, Filipowska A, Fiorino F, Struga M. Anticancer activities of fatty acids and their heterocyclic derivatives. *Eur J Pharmacol*. 2020;15(871):172937.
  45. Chen K, Kurgan L. Investigation of atomic level patterns in protein-small ligand interactions. *PLoS One*. 2009;4(2):e4473.

46. Hendler SS, Sanchez R, Inventors; Biodor US Holding, Vyrex Corp, assignee. Tocopherol-based antiviral agents and method of using same. United States Patent US. 1992;114:957.
47. Harrod KS, Pacl HT, Tipper JL, Ahmad S, Ahmad A, Holder G, Petit C, Green T, Steyn AJC, Might M. Water soluble tocopherol derivatives inhibit the SARS-CoV-2 RNA dependent RNA polymerase. *Am J Respir Crit Care Med*. 2022;205(1):A3610.
48. Burčová Z, Kreps F, Greifová M, Jablonský M, Ház A, Schmidt S, Surina I. Antibacterial and antifungal activity of phytosterols and methyl dehydroabietate of Norway spruce bark extracts. *J Biotechnol*. 2018;20(282):18–24.
49. Rolta R, Salaria D, Sharma P, Sharma B, Kumar V, Rathi B, Verma M, Sourirajan A, Baumler DJ, Dev K. Phytocompounds of rheum emodi, thymus serpyllum, and artemisia annua inhibit spike protein of SARS-CoV-2 binding to ACE2 receptor: in silico approach. *Curr Pharmacol Rep*. 2021;7:135–49.
50. Rolta R, Yadav R, Salaria D, Trivedi S, Imran M, Sourirajan A, Baumler DJ, Dev K. In silico screening of hundred phytocompounds of ten medicinal plants as potential inhibitors of nucleocapsid phosphoprotein of COVID-19: an approach to prevent virus assembly. *J Biomol Struct Dyn*. 2021;39(18):7017–34.
51. Kufareva I, Abagyan R. Methods of protein structure comparison. *Methods Mol Biol*. 2012;857:231–57.
52. Al-Karmalawy AA, Dahab MA, Metwaly AM, Elhady SS, Elkaeed EB, Eissa IH, Darwish KM. Molecular docking and dynamics simulation revealed the potential inhibitory activity of ACEIs against SARS-CoV-2 targeting the hACE2 receptor. *Front Chem*. 2021;4(9):661230.
53. Morris KF, Geoghegan RM, Palmer EE, George M Jr, Fang Y. Molecular dynamics simulation study of AG10 and tafamidis binding to the Val122Ile transthyretin variant. *Biochem Biophys Res*. 2020;17(21):100721.
54. Garcia HG, Kondev J, Orme N, Theriot JA, Phillips R. Thermodynamics of biological processes. *Methods Enzymol*. 2011;492:27–59.
55. Benet LZ, Hosey CM, Ursu O, Oprea TI. BDDCS, the Rule of 5 and drugability. *Adv Drug Deliv Rev*. 2016;1(101):89–98.
56. Sehnert SS. Drug bioavailability: estimation of solubility, permeability, absorption and bioavailability. *J Natl Med Assoc*. 2004;96(9):1243.
57. Prasanna S, Doerksen RJ. Topological polar surface area: a useful descriptor in 2D-QSAR. *Curr Med Chem*. 2009;16(1):21–41.

## Publisher's Note

Springer Nature remains neutral with regard to jurisdictional claims in published maps and institutional affiliations.